Shaping of a scroll wave filament by cardiac fibers

Omer Berenfeld,[1] Marcel Wellner,[1,2] José Jalife,[1] and Arkady M. Pertsov[1]
[1]*Department of Pharmacology, SUNY Upstate Medical University, Syracuse, New York 13210*
[2]*Physics Department, Syracuse University, Syracuse, New York 13244-1130*
(Received 29 November 2000; published 15 May 2001)

Scroll waves of electrical excitation in heart tissue are implicated in the development of lethal cardiac arrhythmias. Here we study the relation between the geometry of myocardial fibers and the equilibrium shape of a scroll wave filament. Our theory accommodates a wide class of myocardial models with spatially varying diffusivity tensor, adjusted to fit fiber geometry. We analytically predict the exact equilibrium shapes of the filaments. The major conclusion is that the filament shape is a compromise between a straight line and full alignment with the fibers. The degree of alignment increases with the anisotropy ratio. The results, being purely geometrical, are independent of details of ionic membrane mechanisms. Our theoretical predictions have been verified to excellent accuracy by numerically simulating the stable equilibration of a scroll filament in a model of the FitzHugh-Nagumo type.

DOI: 10.1103/PhysRevE.63.061901 PACS number(s): 87.19.Hh, 82.40.Ck

I. INTRODUCTION

The heart muscle, seen as an excitable medium, has complex geometrical features that affect its electrophysiological behavior. Prominent among these features is the anisotropy of the constituent fibers. The excitation itself can, in a common pathological case, consist of a scroll wave that rotates about a tubelike self-organizing center known as a filament [1–3]. The present paper is devoted to the effect of fiber shape on filament shape, and is part of a series [4–8] dealing with how and to what extent cardiac geometry governs the configuration of scroll waves, as characterized by their filaments. Our focus is on the fibers' deviation from the straight line; in contrast, our earlier work featured rectilinear fibers with a twist in their orientation. As we shall see, the filament responds somewhat differently to those two kinds of geometry. Whereas the filament was shown to align with the straight fibers, in the present curvilinear-fiber case it adopts a compromise between alignment and the straight-line tendency that results from its effective tension [9]. The extreme cases of very weak and very strong anisotropy will produce rectilinearity and alignment respectively, as one might expect.

The analysis that follows allows much freedom in the assumed fiber shape. Nevertheless, the resulting (and nontrivial) filament shape, if unique, can be predicted without approximation. This is unusual in a nonlinear situation involving a spatially distributed system.

Mathematically, the class of media to be considered is represented by generic models (FitzHugh-Nagumo [10,11], Beeler-Reuter [12], Luo-Rudy [13], or others). We use the standard monodomain formulation, which involves the variable u (the cells' transmembrane potential) and one or more other variables $(v_1, v_2, v_3, \ldots) \equiv \vec{v}$. Their time evolution is given by

$$\partial_t u - \partial_i (D_{ij} \partial_j u) + \Phi(u, \vec{v}) = 0, \tag{1}$$

$$\partial_t \vec{v} + \vec{\Psi}(u, \vec{v}) = 0. \tag{2}$$

Here Φ and $\vec{\Psi}$ are the reaction functions; in our notation we have $\{x_i\} = \{x, y, z\}$, and sums over repeated indices are understood. The diffusivity tensor D has components, given in the next section, that depend on the space coordinates so as to reflect the local fiber direction.

The word ''fiber'' needs a comment. It is a convenient shorthand for visualizing the geometry, in which the fiber or longitudinal direction is that of fastest propagation. On the other hand, in our mathematical description, there will be no identifiable fibers, but only a local fiber direction; see Fig. 1.

In order to determine the equilibrium configuration of the filament, we search for a spatial coordinate transformation that diagonalizes the diffusivity tensor everywhere while avoiding the introduction of convection terms. The purpose is to obtain a new system that supports a steady-state solution with a rectilinear filament. The inverse transformation is then applied, and the straight filament acquires the desired shape. For an illustration of the end result, see Fig. 2.

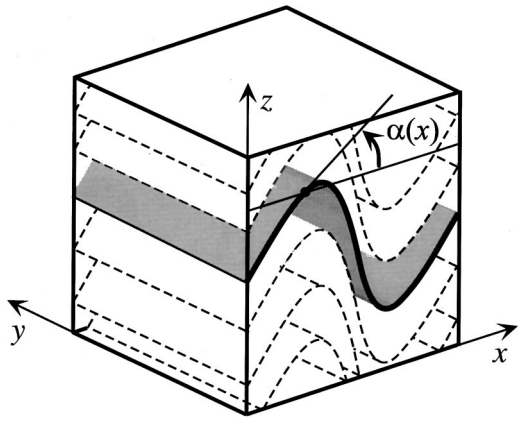

FIG. 1. A slab of excitable medium with the fiber shape displayed as a heavy curve in the xz plane. All fibers are translated versions of that prototypical shape, which happens to be sinusoidal in this illustration. The local fiber slope is defined by the angle $\alpha(x)$ as shown. For application to the heart muscle, we view the z axis as the transmural direction, i.e., approximately perpendicular to the adjacent cardiac surfaces.

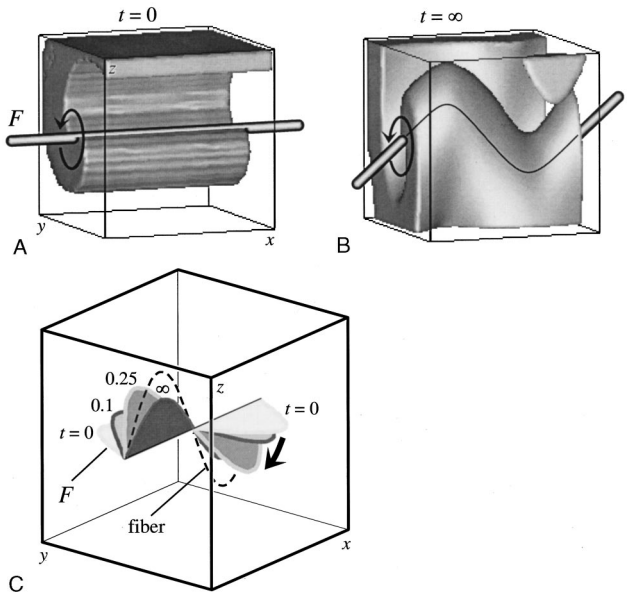

FIG. 2. Equilibration of a scroll wave, under different initial conditions, in the medium of Fig. 1. (a) Initial template, with filament F parallel to the x axis. (b) Starting from the configuration of panel (a), and after about three rotations, the filament has stabilized into a shape fairly similar to that of the fibers shown in Fig. 1. (c) When differently started, the filament (solid curve) evolves toward the same equilibrium state; sequential positions are shown. (The dashed curve represents a typical fiber.) At $t=0$ the filament is sinusoidal in the xy plane. Its approximate plane gradually tilts (arrow) to match the plane of the fibers at equilibrium (t is in seconds). In summary, in our numerical experiments, no matter how the filament is started, its equilibrium shape is the same; however, this shape never quite coincides with the fiber's shape even in the large-time limit.

The purely geometrical nature of the method yields a prediction that is independent of the properties responsible for the medium's excitable behavior. This circumstance confers wide generality to the calculation. Further on in this article, the theory's validity is confirmed numerically in three dimensions. The wave is started with a simple but otherwise arbitrary shape for its filament, and settles quickly into its steady-state mode. All our simulated steady-state scrolls not only agree with the analytic results, but display excellent stability as well, a feature concerning which the theory has nothing to say.

II. GEOMETRY OF THE MODEL

A. The medium

As illustrated in Fig. 1, the prototype fiber is contained in the xz plane; the fiber is given for later convenience by way of its local slope $S(x)$, assumed to be a finite single-valued function. Thus we set

$$z_{\text{fiber}}(x)=\int S(x)dx. \tag{3}$$

All fibers in the xz plane are assumed to be obtained from parallel translation of the prototype in the $\pm z$ direction. Thus, according to the choice of integration constant, Eq. (3) represents any fiber in the plane. We then obtain the fiber geometry of all other planes from parallel translation of the xz plane in the $\pm y$ direction. In summary, all fibers in the medium are versions of the prototype fiber, parallel translated along any direction contained in the yz plane; the medium is invariant with respect to this set of translations; for theoretical purposes it is therefore taken as unbounded in these two directions.

The diffusivity tensor is most simply described in its diagonal form, based on the local fiber orientation,

$$D_{\text{diag}}=\text{diag}(D_L,D_T,D_T). \tag{4}$$

In the above, corresponding to the subscripts L and T, the principal directions are longitudinal, along the local fiber; transverse, in the xz plane perpendicularly to the fiber; and again transverse, parallel to the y axis. (In the heart, D_L is larger than D_T by an order of magnitude.)

In order to obtain the diffusivity components in the xyz frame we apply a rotation about the y direction, designed to achieve the slope S. We find (in terms of the $x_1x_2x_3$ notation)

$$\begin{aligned} D_{11}&=D_L\cos^2\alpha+D_T\sin^2\alpha,\\ D_{22}&=D_T,\\ D_{33}&=D_L\sin^2\alpha+D_T\cos^2\alpha,\\ D_{12}&=D_{21}=D_{23}=D_{32}=0,\\ D_{13}&=D_{31}=(D_L-D_T)\cos\alpha\sin\alpha, \end{aligned} \tag{5}$$

with $\alpha=\alpha(x)$ obtained from

$$\tan\alpha=S \tag{6}$$

[see Eq. (3)]. In D_{ij} we therefore have

$$\begin{aligned} \cos^2\alpha&=1/(S^2+1),\\ \sin^2\alpha&=S^2/(S^2+1),\\ \sin\alpha\cos\alpha&=S/(S^2+1). \end{aligned} \tag{7}$$

Thus we see that the fibers themselves will not enter the mathematics; only their local direction, given by S, is relevant.

B. The wave and filament

While the medium is constructed to be translationally invariant in both the y and z directions, neither of these two invariances is postulated for the excitation wave. Rather, we deal with a genuinely three-dimensional problem in a cube of sides $\Delta x=\Delta y=\Delta z=L$.

The mathematics of this article presupposes the existence of a unique solution for the scroll wave, up to an overall translation parallel to the yz plane. Accordingly, the boundary conditions for the propagating variable u will play a substantive role. For definiteness we assume a single filament

that enters and leaves the cube through the $x=0$ and $x=L$ faces; but uniqueness requires more detail. We can see that in the hypothetical case of a uniform medium, infinite in all directions, including the x direction, uniqueness will break down: the (rectilinear) filament can adopt any direction.

Our choice for avoiding this kind of indeterminacy is to enforce zero-flux boundary conditions across those two planes. Explicitly, considering any point P on a boundary, and if $\mathbf{n}=\{n_1,n_2,n_3\}$ is a vector normal to that boundary at P, then we require

$$n_i D_{ij}\partial_j u=0 \tag{8}$$

at P. In the present case we take $\mathbf{n}=\{1,0,0\}$, so that Eq. (8) reads

$$D_{1j}\partial_j u=0 \quad (x=0,L). \tag{9}$$

In all the following theory and simulations we shall make that assumption. The boundary conditions at the remaining four cube faces will be ignored in the analytical work. That is, the medium is deemed to be effectively infinite in the $\pm y$ and $\pm z$ directions. Simulations must, of course, implement this with a large enough cube size.

As regards the filament, we shall define it in terms of the variables u and $\vec{v}$ in Eqs. (1) and (2). We plot the instantaneous intersection of chosen contours for two variables, say u and v_1, thus obtaining a periodically shifting curve that delineates a narrow filament tube over time.

III. A SPECIAL DIAGONALIZATION

Let the diffusion operator in Eq. (1) be written in ''explicit'' form as $\partial_i(D_{ij}\partial_j)=D_{ij}\partial_i\partial_j+E_i\partial_i$ for some E_i, where $E_i\partial_i$ is the convective part of the operator. We look for a transformation T of the spatial coordinates $(x,y,z)\rightarrow(X,Y,Z)$ such that (a) the diffusivity tensor becomes diagonal, and (b) the explicit transformed operator has no convective terms in the transverse directions Y or Z, i.e., no terms of the form $P\partial_Y$ or $Q\partial_Z$. Such terms are known to cause a drift of the filament [7,14, and references therein], and thus are incompatible with the steady state. If convection is absent, and because of the new medium's symmetries about the X axis, we expect the existence of a stationary scroll with a rectilinear filament in the X direction. For weak enough curvature of the fibers, the existence of that scroll is guaranteed by continuity. Indeed, with straight fibers we have uniform anisotropy, which is known to support a straight filament. For stronger (and sometimes very strong) curvatures, our computer simulations still demonstrate the existence of the expected scroll.

Naively, the problem might seem trivial. We have obtained the actual diffusivity tensor (5) from its diagonal form (4) through a local rotation. Why not simply invert that rotation? The main reason is that it cannot usually be done even in principle. Although a diffusion tensor can be locally rotated, a coordinate system in general cannot: two neighboring local rotations are in general incompatible.

On a less abstract level, we note that, although Eq. (4), with physical eigenvalues, is unique apart from exchanges of coordinate axes, the diagonalization condition can be accomplished by other than a pure rotation if we allow the eigenvalues to become formally dependent on (X,Y,Z). The condition of no transverse convection will determine which diagonalization process to choose.

We consider candidates from the following class of transformations $(x,y,z)\rightarrow(X,Y,Z)$:

$$X=x, \quad Y=y,$$

$$Z=z-\int^S f(S)dS=z-\int^x f(S)S'(x)dx, \tag{10}$$

where the function f is as yet undetermined. This working assumption, which severely restricts the set of available transformations, is motivated in part by the simplicity of what follows, but ultimately by the fact that it will lead to the appropriate diagonalization T. [We observe that a naive straightening of the fibers, $Z_{\rm str}=z-\int S(x)dx$, cf. Eq. (3), although inappropriate, is similar to Eq. (10) in regard to separation of coordinates.] With Eqs. (10), the partial derivatives now read

$$\partial_x=\partial_X-f(S)S'(X)\partial_Z, \quad \partial_y=\partial_Y, \quad \partial_z=\partial_Z, \tag{11}$$

where the prime denotes the ordinary derivative.

We next look at the complete diffusion operator in Eq. (1). In the XYZ system, this operator can be written generically as

$$\partial_i(D_{ij}\partial_j)=A_{XX}\partial_X^2+A_{XZ}\partial_X\partial_Z+A_{ZZ}\partial_Z^2+A_{YY}\partial_Y^2+B_X\partial_X+B_Z\partial_Z. \tag{12}$$

[In consequence of the particular spatial dependence set out in Eq. (5), there is no ∂_Y term, and we still have $A_{YY}=D_T$.] In general, the A and B coefficients are expected to depend on position; as mentioned previously, however, we need to determine $f(S)$ so as to enforce

$$A_{XZ}=0, \quad B_Z=0. \tag{13}$$

By inserting Eqs. (11) into $\partial_i(D_{ij}\partial_j)$, we obtain the coefficients in Eq. (12). Specifically, we have

$$A_{XZ}=\frac{2}{S^2+1}[-(D_L+D_TS^2)S'f(S)+(D_L-D_T)S]. \tag{14}$$

Requiring this to vanish yields

$$f(S)=\frac{(D_L-D_T)S}{(D_L+D_TS^2)S'}, \tag{15}$$

or else the trivial case $S=S'=0$. Similarly, we have

$$B_Z=\partial_X\left(\frac{R}{S^2+1}\right), \tag{16}$$

where

$$R=-(D_L+D_TS^2)S'f(S)+(D_L-D_T)S, \tag{17}$$

proportional to A_{XZ}, Eq. (14). Remarkably, therefore, we find $R=0$, or $B_Z=0$. Thus, the transformations of type (10) have the desirable property that, together with the diagonalization requirement $A_{XZ}=0$, they automatically ensure the absence of convection terms perpendicular to the X axis. In summary, Eq. (12) has the surviving terms

$$\partial_i(D_{ij}\partial_j)=A_{XX}\partial_X^2+A_{ZZ}\partial_Z^2+D_T\partial_Y^2+B_X\partial_X, \tag{18}$$

where all coefficients are independent of Y and Z. This formula is as far as we shall need to carry the diagonalization procedure. For completeness we nevertheless list the explicit forms of A_{XX}, A_{ZZ}, and B_X:

$$A_{XX}=\frac{D_L+D_TS^2}{S^2+1},$$

$$A_{ZZ}=\frac{D_LD_T(S^2+1)}{D_L+D_TS^2}, \tag{19}$$

$$B_X=-\frac{2(D_L-D_T)SS'}{(S^2+1)^2}.$$

To conclude this section we must address the boundary conditions in the XYZ medium. We have eliminated any Y or Z dependence in the transformed diffusivity components. Therefore any residual perturbation in a lateral direction would have to be caused by the boundary conditions, in particular Eq. (9). With the help of Eqs. (5) and (7), that condition reads

$$[(D_L+D_TS^2)\partial_x+(D_L-D_T)S\partial_z]u=0. \tag{20}$$

After applying transformation (11) we find that the ∂_Z coefficient is again proportional to A_{XZ} in Eq. (14), and thus vanishes, while the ∂_X coefficient is nonzero. This leaves us with

$$\partial_X u=0 \quad (X=0,L), \tag{21}$$

symmetric in the transverse directions. In summary, the usual fiber-adapted no-flux conditions in the actual xyz system preserve the Y and Z symmetry of the conditions in XYZ space, at least along the boundary planes $X=0,L$.

The same cannot be said of no-flux conditions at the lateral boundaries (along $Y=\text{const}$ or $Z=\text{const}$). Instead we theoretically assume a medium infinite in the Y and Z directions; in simulations we must then set up the scroll wave with its filament ''not too close'' to the lateral boundaries; experience shows that one or two scroll windings amount to a safe distance.

IV. SHAPE OF THE FILAMENT

In this section we first demonstrate that, based on the form (18), the filament in the XYZ system is indeed rectilinear, in the X direction, and stationary. To that end we present a constructive definition of a stationary filament. Rectilinearity and the X direction are simultaneously deduced from the symmetries of the transformed medium and from the postulate that the equilibrium shape and orientation of the filament are unique. Readers may wish to skip these mathematical preliminaries and go over directly to the second part of the section, where we obtain the actual filament shape by means of the inverse transformation back to the original coordinate system.

A. A unique rectilinear filament in XYZ space

From the new medium's symmetry about the X axis, as displayed in Eq. (18), the filament in the XYZ system might be expected intuitively to be rectilinear and in the X direction. However, the actual filament may have a complicated and spatially variable cross section due to the residual X dependence of the medium, and, in addition, it may exhibit helical features due to the scroll's chirality. We now construct a filament axis that does indeed turn out to be linear and in the X direction.

From Eqs. (18) and (20), the medium, including its boundary conditions, is invariant under each reflection $Y\rightarrow -Y$ and $Z\rightarrow -Z$, as well as under all translations in the YZ plane. We shall be interested in the effect of these transformations on the filaments of scroll wave solutions that are periodic in time, and whose existence we postulate.

As a help in constructing the filament tube, we assume that when a scroll is sectioned parallel to the YZ plane the result is a spiral that rotates (not necessarily rigidly) in a clockwise (CW) or counterclockwise (CCW) direction according to some convention, thus defining two classes, the CW and CCW scrolls. For any scroll, a filament tube can now be constructed on the basis of two selected variables, say u and v_1. At any given time and in any given YZ section, we define a point F that is the intersection of two contour lines $u=\mu, v_1=\nu$ (μ and ν are chosen constants). Let C be the spatial orbit of F over a complete cycle. We similarly construct the corresponding C, with the same μ and ν, in every YZ section, and regard the combined set of all closed curves C as the filament tube. By construction, this tube is of course independent of time.

Before we proceed to derive the filament shape, a further assumption is needed: If the direction of rotation, CW or CCW, as well as the ''filament labels'' (μ,ν) are given, then the filament tube is unique up to translations in the YZ plane. The consequences of doing without that assumption are taken up in Appendix B.

We now improve the characterization of the filament by going over from filament tube to filament axis. Consider, for example, a CW filament tube, and apply the combined reflections $Y\rightarrow -Y, Z\rightarrow -Z$. The result is still a CW filament tube, and from the uniqueness assumption it follows that we now have recovered the original filament tube, but translated in the YZ plane. The translation vector depends on where the origin of the YZ plane is located relative to the original tube. For example, if that origin lies within the tube, the amount of translation is expected to be very small. We now shift the YZ origin (two free parameters) until the two-dimensional trans-

lation vector vanishes. The new X axis is then defined to be the filament axis. In summary, the filament axis is a line parallel to the X axis, such that a central YZ reflection about it reproduces the filament tube without translation. Our construction has demonstrated the existence of the filament axis.

B. Filament shape in *xyz* space

In order to return to the original xyz system, we select a (necessarily rectilinear) filament axis, say $Y=Z=0$. Equations (10) then yield the desired filament shape,

$$y_{\text{filament}}=0, \quad z_{\text{filament}}=\int^{S} f(S)dS=\int^{x} f(S)S'dx, \quad (22)$$

where the function $S=S(x)$ is considered given. Explicitly, from Eq. (15), we have

$$z_{\text{filament}}=(D_L-D_T)\int^{x}\frac{Sdx}{D_L+D_TS^2}. \quad (23)$$

This formula, which concludes our mathematical analysis, predicts the shape of a curved filament ''axis'' in a medium whose fiber is given by Eq. (3). A more intuitive version of Eq. (23) displays the filament's slope S_{filament} in terms of the fiber's slope S and the inverse anisotropy ratio $\rho=D_T/D_L$ $(0<\rho<1)$:

$$S_{\text{filament}}=\left(\frac{1-\rho}{1+\rho S^2}\right)S. \quad (24)$$

We have here the central result of our work, stating that the filament adopts a local slope that is always less than that of the fiber. Therefore Eq. (24) implies that the filament has an overall shape which is a compromise between that of the fiber and the x axis. (The x axis configuration would be the filament shape in a uniform isotropic medium, $\rho=1$, under our no-flux boundary conditions at $x=0,L$.) In the limit $D_L/D_T\to\infty$ $(\rho=0)$, the filament approaches the fiber in terms of shape and orientation. The dependences of S_{filament} on S and on ρ are separately of considerable interest, and are plotted in Fig. 3. For each value of ρ, the nonmonotonicity as a function of S should be noted. It allows us to predict that, where the fiber is steep enough (at the right of the peak), the filament will follow the fiber less closely as the fiber slope increases.

The uniqueness of the solution has played a role in our derivation. Genuine cases of nonuniqueness may in principle exist, however. For example, the filament shape could bifurcate into a pair of possibilities, both different from Eq. (23). One member of the pair is then predictable in terms of the other, as we show in Appendix B. We have seen no such occurrence in our simulations.

V. NUMERICAL ILLUSTRATIONS

The predictions of Eq. (23) are confirmed by the numerical simulations of stable scrolls. These are based on a FitzHugh-Nagumo-type model whose details are set out in Appendix A.

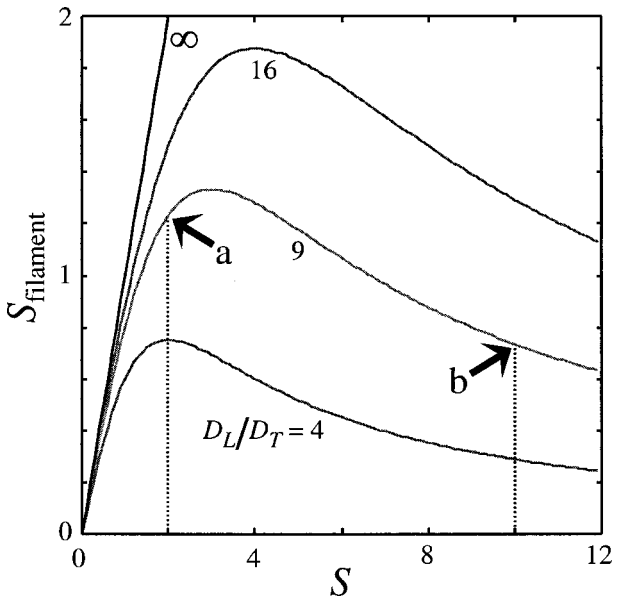

FIG. 3. Filament slope against fiber slope for different anisotropies according to formula (24). With increasing anisotropy, the local filament slope increases. Points a and b refer to the results of Fig. 5 further on. The curve labeled ''∞'' is where filament and fiber slopes coincide.

In Figs. 2(A) and 2(B) we show how the scroll evolves from rectilinear at initiation to a shape rather similar to that of the fibers. Panel (A) shows the initial scroll with its rectilinear filament. This configuration (stable in uniform isotropic media) becomes unstable when the fibers are curved. Panel (B) shows the scroll after the filament has reached an equilibrium determined by the fibers of Fig. 1.

Figure 2(C) displays the equilibration process for another choice of initial conditions. Unlike the scenario that begins in Fig. 2(A) with a straight filament and takes place entirely within the xz plane, here the initial filament is chosen to be a curve that resides in the xy plane. After about 1.5 scroll rotations ($t=0.1$ in the figure), the approximate plane of the filament is already seen to be substantially rotated as well. It continues to rotate toward the plane of the fibers (the xz plane), along which it stabilizes with the same stationary filament configuration as in Fig. 2(B), in accordance with theory.

Figure 4 illustrates the earlier-mentioned effect of the anisotropy D_L/D_T on the degree of alignment. Equation (24), when written in terms of the inverse of that ratio, shows a fiber-filament alignment that improves with increasing D_L/D_T. The left panel of Fig. 4 shows the analytical filament solutions for three anisotropy ratios (16, 9, and 4): the higher the anisotropy, the closer the alignment. We now select a fiber whose average z coordinate is equal to that of the filament. The maximal deviation Δ between filament and fiber is then taken as a measure of misalignment. In the right panel we plot Δ as a function of the anisotropy to demonstrate how alignment improves with anisotropy. The computational results are superimposed for comparison. Under

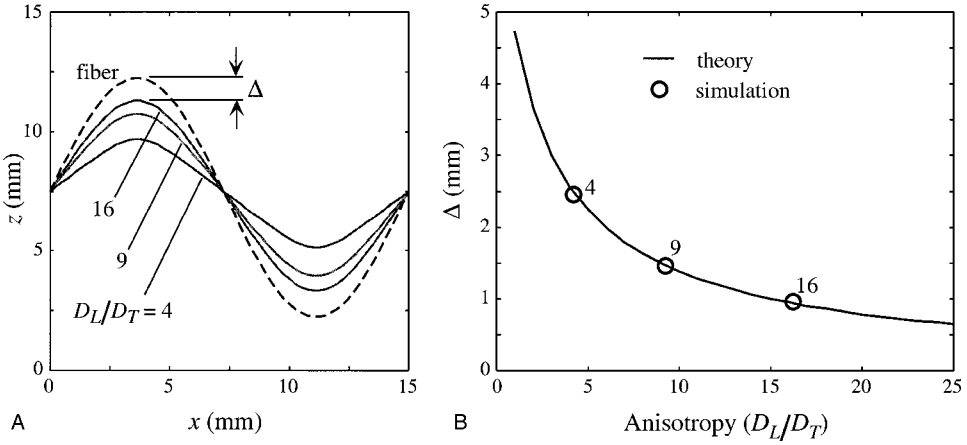

FIG. 4. Effect of increasing the anisotropy. (a) Analytical solutions (solid curves) for three different anisotropy ratios; the dashed curve is the fiber shape. As the anisotropy ratio increases from 4 to 16, the alignment improves, decreasing the difference Δ between the amplitudes of fiber and filament. (b) The difference Δ, as a function of the anisotropy ratio D_L/D_T. The numerical results (circles) for $D_L/D_T=4$, 9, and 16 are seen to coincide with the prediction (curve). Full alignment ($\Delta=0$) is predicted in the strong-anisotropy limit $D_L/D_T\rightarrow\infty$.

strong anisotropy, as in cardiac muscle ($D_L/D_T\simeq 9$), a rather good alignment should prevail everywhere.

The excellent agreement between theory and numerical solution is demonstrated in Fig. 5 for different fiber shapes. In each of these three cases [panels (A), (B), and (C)] we plot the stationary filament from the numerical scroll wave simulation, and trace for comparison the analytically predicted filament, as well as one layer of the actual fibers. Note that the alignment is less perfect for segments with extreme slope. This circumstance finds its explanation in the nonmonotonic curves of Fig. 3, where we plot the theoretical filament slope against the fiber slope for various degrees of anisotropy. The small bumps exhibited in the inset of Fig. 5(B) are a special confirmation of the theory. Panel (C) of Fig. 5 illustrates a medium with piecewise linear fibers. This unphysiological shape, with its sharp corners, puts the theory to a severe test. Nevertheless, and remarkably, the simulated scroll rotates around a piecewise linear filament complete with sharp corners. The curvature at these corners is of course not well defined for either the fiber or the filament.

VI. DISCUSSION

The major result of this study is that the filament of a scroll wave tends to align with the fibers in the excitable medium and that, for given boundary conditions, the degree of alignment depends on the anisotropy ratio in a quantitatively predictable manner. Analytically, this result amounts to the pair of equations (3) and (23), which prescribe the shape of a scroll filament in a given fiber configuration of the medium. The numerical illustrations of the preceding section are in excellent agreement with that theory, sometimes to a striking degree, as when the fibers involve sharp corners.

Partial alignment can be expected from the following qualitative argument. On the one hand, it was found in the case of twisted anisotropy [6,14] that rectilinear filaments move into alignment with the (rectilinear) fibers; on the other hand, under isotropic conditions, and when the excitability of the medium is not too low, filaments ''attempt'' to minimize their length as though they were under mechanical tension [9]. When the fibers are curved, these two tendencies are incompatible, and Fig. 5 displays a clear compromise between them. The degree of anisotropy tilts the balance one way or the other, and, as implied by formula (24), an infinitely strong anisotropy $D_L/D_T\rightarrow\infty$ yields perfect alignment.

How generally should we expect the present results to hold? Our argument is purely geometrical and distinct from the specific ionic mechanisms of excitation. Therefore the choice of membrane model is not critical to the validity of our results. The time-dependent details of the approach to equilibrium do, however, depend on the specifics of the model and may vary with its parameters. That time dependency is interesting in it own right, and in general can be learned only from numerical simulations as of now. Although the theory leads to a well-defined equilibrium configuration, it has, in its present form, nothing to say about stability, which may well be model dependent. (In the numerically tested cases the stability has been excellent.)

We now turn to some cardiological considerations. Scroll waves are considered a major mechanism of severe ventricular arrhythmias [1–3,15–18]. Unfortunately, owing to the limitations of present techniques, scrolls are very poorly documented in living tissue as far as their three-dimensional organization is concerned. Here we have supplied analytical and computational evidence to guide our expectations.

The approximate alignment that our studies have found under a wide range of conditions is one way to understand the relatively rare observation of sustained spiral waves on the ventricular epicardium. The spirals would be nothing but short-lived manifestations of transmural (rather than intramural, i.e., fiber-aligned) scrolls [19–21]. Such an interpretation is consistent with quite a number of multiple-electrode studies [22–24,17,18], and would confirm the likely role of scroll waves in the maintenance of cardiac arrhythmias. Alternatively, a possible instability of the scroll itself (rather

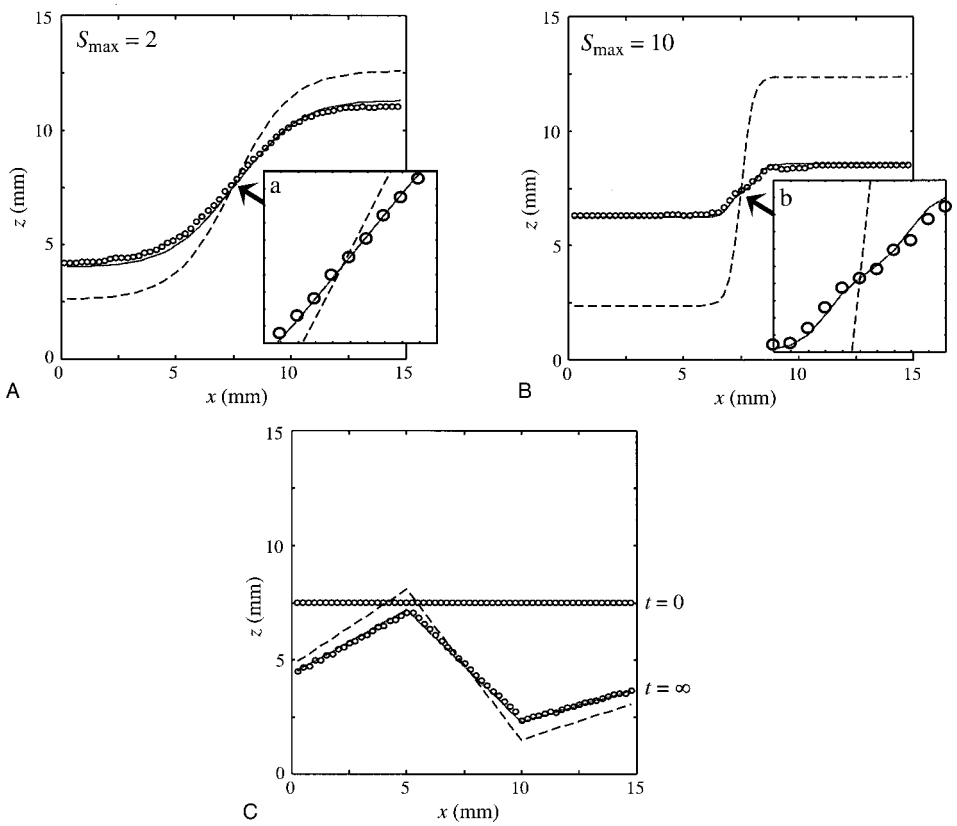

FIG. 5. Theoretical and simulated filaments for different fiber shapes, all with $D_L/D_T = 9$. (Curves and points have the same meaning as in previous figures.) The small bumps visible in the inset of (b) but not of (a) are due to the nonmonotonicity of the curves in Fig. 3; points a and b in the earlier Fig. 3 refer to the present insets. As the fiber in (b) goes through its steepest region, its slope of around 10, plotted horizontally in Fig. 3, goes back and forth through the peak region. In contrast, the slope in (a) has maximum value 2, and therefore never becomes steep enough for a crossing of the peak region. The bumps, while far from spectacular in themselves, are the only fine structure we see in an otherwise smooth landscape, and thus they are a powerful confirmation for the theory. Note the excellent agreement between simulations (circles) and theory (solid curves). Panel (c) displays the remarkable persistence of this agreement even when the fibers are (unphysiologically) piecewise linear. In (c), the filament was started as a horizontal line at $z = 7.5$ mm, but has drifted substantially downward before stopping at its final location. This phenomenon, which in no way conflicts with our theory, is permitted by the asymmetry of the fibers with respect to a 180° rotation in the xz plane.

than the orientation of its filament) is emphasized in [1].

In earlier computer simulations using a realistic whole-heart model, some of us [25] have demonstrated the presence of stable filaments curled around the ventricular apex and following the gross anatomical fiber direction [26–28]. The present study provides an explanation for such configurations.

ACKNOWLEDGMENTS

Our work was supported by Grant Nos. PO1-HL-39707 and RO1-HL-60843 from the National Heart, Lung, and Blood Institute of the National Institutes of Health.

APPENDIX A: THE MODEL

We simulate a $15\times15\times15$ mm^3 ventricular free-wall slab with curved fibers parallel to each other. The fibers' shape is obtained by varying their slope angle α along x. Three different geometries are used.

(1) Sine-wave shaped fibers,

$$z_{\text{fiber}}(x) = A\sin(2\pi x/L), \tag{A1}$$

where L is the size of the slab and $A = 5$ mm.

(2) Hyperbolic-tangent shaped fibers,

$$z_{\text{fiber}}(x) = A\tanh k(x - L/2), \tag{A2}$$

where L and A are as in Eq. (A1) and k is used to adjust the slope.

(3) Piecewise linearly shaped fibers,

$$z_{\text{fiber}}(x) = \begin{cases} \dfrac{2A}{L}x & \text{for} \quad 0 \leqslant x < a, \\ \dfrac{A}{L}(6a - 4x) & \text{for} \quad a \leqslant x \leqslant 2a, \\ \dfrac{A}{L}(x - 4a) & \text{for} \quad 2a < x \leqslant L, \end{cases} \tag{A3}$$

where A and L are the same as in the sine wave fibers, and $a = L/3$. The construction of the slab consists of obtaining

analytically the slopes $S(x)$ of the fibers and the angle $\alpha(x)$, and then rotating the diffusion tensor D as described by Eq. (5).

The action potential is simulated using FitzHugh-Nagumo (FHN) type equations in the form described by Eqs. (1) and (2) with a one-element $\vec{v} \equiv v, \vec{\Psi} \equiv \Psi$ (see also Ref. [29]); u is the transmembrane potential and v is the variable that controls the currents. The reaction functions $\Phi(u,v)$ and $\Psi(u,v)$ are

$$\Phi(u,v) = \begin{cases} v + 20u & \text{for} \quad u < u_1, \\ v - 3u + 0.15 & \text{for} \quad u_1 \leqslant u < u_2, \\ v + 15(u-1) & \text{for} \quad u_2 \leqslant u. \end{cases} \tag{A4}$$

$$\Psi(u,v) = \begin{cases} (v-3u)/5 & \text{for} \quad u < u_1, \\ (v-3u)/15 & \text{for} \quad u_1 \leqslant u < u_2, \\ (v-3u)/5 & \text{for} \quad u_2 \leqslant u. \end{cases} \tag{A5}$$

For the continuity of the piecewise linear $\Phi(u,v)$ we set $u_1 = 0.15/23$ and $u_2 = 15.15/18$.

We impose no-flux (homogeneous Neumann) boundary conditions of the form

$$n_i D_{ij} \partial_j u = 0 \tag{A6}$$

[in the notation of Eq. (1)], where the n_i are the Cartesian components of the unit vector **n**, normal to the xy, xz, and yz boundary planes. Thus, in component form, the boundary conditions read

$$D_{11}\partial_x u + D_{13}\partial_z u = 0 \quad (x = 0, L), \tag{A7}$$

$$\partial_y u = 0 \quad (y = 0, L), \tag{A8}$$

$$D_{31}\partial_x u + D_{33}\partial_z u = 0 \quad (z = 0, L). \tag{A9}$$

The initial wave is chosen by way of template functions $u(x,y,z), v(x,y,z)$. For simplicity, the initial filament is rectilinear and parallel to the x axis in all cases except in Fig. 2(C), where it is sinusoidal and lies in the xy plane. It is always positioned in the middle of the slab.

We integrate the set of Eqs. (1) and (2) using the explicit Euler method. All derivatives are calculated as standard central differences. The lattice size is $60 \times 60 \times 60$ elements. The model is scaled to achieve a physiologically reasonable propagation velocity of 0.5 m/s (in the fastest direction) and a rotational period of about 70 ms. In the majority of simulations, the spatial discretization step is $h = 0.2$ in all directions and the time step $\Delta t = 0.01$. Both values are close to those normally used in FHN simulations [30,31]. In dimensional units, they correspond to 0.25 mm and 0.047 ms, respectively. The convergence of the numerical solutions has been tested in control runs with a refined mesh of $h = 0.1$ and $\Delta t = 0.0025$.

APPENDIX B: NONUNIQUE SOLUTIONS

Our simulations have not demonstrated any cases of nonuniqueness, even if the fibers deviate strongly from the straight line. However, since uniqueness was an important assumption of Sec. IV, and since an anomalous equilibrated filament may correspond to alternative and unsuspected basins of attraction relative to initial conditions, we devote this Appendix to the hypothetical situation where the uniqueness assumption breaks down. In that case Eq. (23) can no longer be expected to hold. Instead, the filament should have an ''anomalous'' shape; we shall see that anomalous filaments must occur in pairs. While we give no *a priori* calculation for both members of the pair, we do (nontrivially) predict one member exactly when the other is known.

The discussion is most conveniently conducted from within the symmetric XYZ system, as obtained through transformation (10), with $S(x)$ still equal to the fibers' slope, Eq. (3). We ask what happens when, in the symmetric XYZ system, the equilibrium filament tube is no longer axially symmetric around any line parallel to the X axis. (Such a spontaneously broken symmetry could arise when the stationary symmetric solution is unstable or nonexistent.) Because the XYZ system is itself symmetric, a double reflection $Y \to -Y, Z \to -Z$ will turn the nonsymmetric filament tube into another physically realizable one, with a distinct reflected shape. Hence, going back to the xyz system, we obtain two different possible filament shapes, neither of which follows Eq. (23). More generally, we see that nonunique filaments will occur in pairs [with, in addition, the solution of Eq. (23) if available]. In what follows we pursue in some detail the question of predicting the exact shape of the second possible filament when the first one has been measured. We keep in mind the practical diagnosis for nonuniqueness: when the observed equilibrium filament violates Eq. (23), we are led to search for its counterpart.

To reach an explicit formula, we start from a steady-state scroll wave solution $\mathcal{U} \equiv \{u, \mathbf{v}\}$ in the original system, and assume that it has the coordinate dependence $\mathcal{U} = \mathcal{U}(x,y,z,t)$. We also assume that its filament does not obey Eq. (23). Therefore we look for a second, different, steady-state scroll $\mathcal{U}^* = \mathcal{U}^*(x,y,z,t)$, obeying the same propagation equations, with the same diffusivity tensor and boundary conditions. We now determine $\mathcal{U}^*$ when $\mathcal{U}$ is known. The method is to apply three successive transformations to $\mathcal{U}$.

(a) Going over to the symmetric XYZ system, gives the transformed function

$$\mathcal{U}_T(X,Y,Z,t) = \mathcal{U}\left(X, Y, Z + \int^X f(S) S'(X) dX, t\right); \tag{B1}$$

see Eq. (10).

(b) Applying the reflections $Y \to -Y, Z \to -Z$ will give another, distinct, solution

$$\mathcal{U}_T^*(X,Y,Z,t) = \mathcal{U}\left(X, -Y, -Z + \int^X f(S) S'(X) dX, t\right). \tag{B2}$$

(c) Transforming back to the xyz system, again using Eq. (10) and then Eq. (15) gives

$$\mathcal{U}^*(x,y,z,t)=\mathcal{U}\left(x,-y,-z+2\int^x f(S)S'(x)dx,t\right)$$
$$=\mathcal{U}\left(x,-y,-z+2\int^x\frac{(D_L-D_T)Sdx}{D_L+D_TS^2},t\right). \quad \text{(B3)}$$

The above is the explicit construction of the second solution $\mathcal{U}^*$.

The corresponding anomalous filament shape is obtained as follows. (Here we can no longer use the symmetry property that defined a filament line—the X axis—in the unique case. However, we can use some other recipe like a time average of the point F that describes the filament tube at all fixed values of X.)

Suppose the first anomalous shape is given parametrically in x by the functions $y_{\text{filament}}(x)$ and $z_{\text{filament}}(x)$, where we note that the filament is no longer necessarily confined to the xz plane. Then, directly from Eq. (B3), we have

$$y^*_{\text{filament}}(x)=-y_{\text{filament}}(x),$$
$$z^*_{\text{filament}}(x)=-z_{\text{filament}}(x)+2\int^x\frac{(D_L-D_T)Sdx}{D_L+D_TS^2}. \quad \text{(B4)}$$

These starred functions give the second anomalous filament explicitly in terms of the first.

[1] F. Fenton and A. Karma, Chaos **8**, 20 (1998).
[2] A. V. Holden and A. V. Panfilov, in *Modelling Propagation in Excitable Media*, edited by A. V. Panfilov and A. V. Holden (John Wiley and Sons, New York, 1997).
[3] A. M. Pertsov and J. Jalife, in *Cardiac Electrophysiology from Cell to Bedside*, 3d ed., edited by D. P. Zipes and J. Jalife (W. B. Saunders, Philadelphia, 1999).
[4] M. Vinson, A. M. Pertsov, and J. Jalife, Physica D **72**, 119 (1993).
[5] A. M. Pertsov and M. Vinson, Philos. Trans. R. Soc. London, Ser. A **347**, 687 (1994).
[6] O. Berenfeld and A. M. Pertsov, J. Theor. Biol. **199**, 383 (1999).
[7] M. Wellner, O. Berenfeld, and A. M. Pertsov, Phys. Rev. E **61**, 1845 (2000).
[8] A. M. Pertsov, M. Wellner, and J. Jalife, Phys. Rev. Lett. **84**, 2738 (2000).
[9] V. N. Biktashev, A. V. Holden, and H. Zhang, Philos. Trans. R. Soc. London, Ser. A **347**, 611 (1994).
[10] R. FitzHugh, Biophys. J. **1**, 445 (1961).
[11] J. Nagumo, Proc. IRE **50**, 2061 (1962).
[12] G. Beeler and H. Reuter, J. Physiol. (London) **268**, 963 (1989).
[13] C. H. Luo and Y. Rudy, Circ. Res. **74**, 1071 (1993); **74**, 1097 (1993).
[14] M. Wellner, A. M. Pertsov, and J. Jalife, Phys. Rev. E **59**, 5192 (1999).
[15] A. B. Medvinsky, A. V. Panfilov, and A. M. Pertsov, in *Self-Organization: Autowaves and Structures Far from Equilibrium*, edited by V. I. Krinsky (Springer-Verlag, Berlin, 1984), pp. 195–199.
[16] A. T. Winfree, Science **266**, 1003 (1994).
[17] S. M. Pogwizd and P. B. Corr, Circ. Res. **66**, 672 (1990).
[18] N. El-Sherif, E. B. Caref, and M. Restivo, Circ. Res. **79**, 474 (1996).
[19] R. A. Gray, J. Jalife, A. V. Panfilov, W. T. Baxter, C. Cabo, J. M. Davidenko, and A. M. Pertsov, Science **270**, 1222 (1996).
[20] R. A. Gray, A. M. Pertsov, and J. Jalife, Nature (London) **392**, 75 (1998).
[21] F. X. Witkowski, L. J. Leon, P. A. Penkoske, W. R. Giles, M. L. Spano, W. L. Ditto, and A. T. Winfree, Nature (London) **392**, 78 (1998).
[22] M. J. Janse, F. J. L. van Capelle, H. Morsink, A. G. Kleber, F. Wilms-Schopman, R. Cardinal, C. N. D'Alnoncourt, and D. Durrer, Circ. Res. **47**, 151 (1980).
[23] P. S. Chen, P. D. Wolf, E. G. Dixon, N. D. Danieley, D. W. Frazier, W. M. Smith, and R. E. Ideker, Circ. Res. **62**, 1191 (1988).
[24] D. W. Frazier, P. D. Wolf, J. M. Wharton, A. S. L. Tang, W. M. Smith, and R. E. Ideker, J. Clin. Invest. **83**, 1039 (1989).
[25] O. Berenfeld and J. Jalife, Circ. Res. **82**, 1063 (1998).
[26] P. M. F. Nielsen, I. J. LeGrice, B. H. Smaill, and P. J. Hunter, Am. J. Physiol. **260**, H1365 (1991).
[27] D. D. Streeter, in *Handbook of Physiology*, edited by R. M. Berne, N. Sperelakis, and S. R. Geigert (American Physiological Society, Bethesda, MD, 1979), pp. 61–112.
[28] I. J. LeGrice, B. H. Smaill, L. Z. Chai, S. G. Edgar, J. B. Gavin, and P. J. Hunter, Am. J. Physiol. **269**, H571 (1995).
[29] A. V. Panfilov and A. M. Pertsov, Dokl. Akad. Nauk SSSR **274**, 1500 (1984) [Sov. Phys. Dokl. **29**, 58 (1984)].
[30] D. Barkley, in *Waves and Patterns in Chemical and Biological Media*, edited by H. L. Swinney and V. I. Krinsky (Elsevier Science Publishers B. V., Amsterdam, 1991), pp. 61–70.
[31] A. V. Panfilov and J. P. Keener, Physica D **84**, 545 (1995).